CONSTRAINING THE ASSEMBLY OF NORMAL AND COMPACT PASSIVELY EVOLVING GALAXIES FROM REDSHIFT $Z = 3$ TO THE PRESENT WITH CANDELS [1]

P. Cassata[2], M. Giavalisco[3], C. C. Williams[3], Yicheng Guo[4], Bomee Lee[3], A. Renzini[5], H. Ferguson[6], S. F. Faber[4], G. Barro[4], D. H. McIntosh[7], Yu Lu[8], E. F. Bell[9], D. C. Koo[4], C. J. Papovich[10], R. E. Ryan[6], C. J. Conselice[11] N. Grogin[6], A. Koekemoer[6], N. P. Hathi[12]

Draft version March 11, 2018

ABSTRACT

We study the evolution of the number density, as a function of the size, of passive early–type galaxies with a wide range of stellar masses ($10^{10}M_\odot < M_* \lesssim 10^{11.5}M_\odot$) from $z \sim 3$ to $z \sim 1$, exploiting the unique dataset available in the GOODS–South field, including the recently obtained WFC3 images as a part of the Cosmic Assembly Near–infrared Deep Extragalactic Legacy Survey (CANDELS). In particular, we select a sample of $\sim$107 massive ($M_* > 10^{10}M_\odot$), passive ($SSFR < 10^{-2}Gyr^{-1}$) and morphologically spheroidal galaxies at $1.2 < z < 3$, taking advantage of the panchromatic dataset available for GOODS, including VLT, CFHT, Spitzer, Chandra and HST ACS+WFC3 data. We find that at $1 < z < 3$ the passively evolving early–type galaxies are the reddest and most massive objects in the Universe, and we prove that a correlation between mass, morphology, color and star–formation activity is already in place at that epoch. We measure a significant evolution in the mass–size relation of passive early–type galaxies (ETGs) from $z \sim 3$ to $z \sim 1$, with galaxies growing on average by a factor of 2 in size in a 3 Gyr timescale only. We witness also an increase in the number density of passive ETGs of 50 times over the same time interval. We find that the first ETGs to form at $z \gtrsim 2$ are all compact or ultra–compact, while normal sized ETGs (meaning ETGs with sizes comparable to those of local counterparts of the same mass) are the most common ETGs only at $z < 1$. The increase of the average size of ETGs at $0 < z < 1$ is primarily driven by the appearance of new large ETGs rather than by the size increase of individual galaxies.

Subject headings: cosmology: observations — galaxies: fundamental parameters — galaxies: evolution

1. INTRODUCTION

Early–type galaxies have been the objects of many studies in the recent years, as they contain crucial information about the evolution of the galaxy content. First, they are by definition the oldest objects at each epoch, and they can be considered relics of the star formation activity that happened in the past; the age of the stellar populations in these galaxies at $z \sim 0$ are compatible with redshifts of formations $z > 2$ (Renzini 2006). Second, early–type galaxies are the most massive objects in the local Universe, containing the bulk of the stellar mass (Baldry et al. 2004).

[1] paolo.cassata@oamp.fr
[2] Aix Marseille Université, CNRS, LAM (Laboratoire d'Astrophysique de Marseille) UMR 7326, 13388, Marseille, France; paolo.cassata@oamp.fr
[3] Department of Astronomy, University of Massachusetts, Amherst, MA 01003
[4] UCO/Lick Observatory, Department of Astronomy and Astrophysics, University of California, Santa Cruz, CA, USA
[5] Osservatorio Astronomico di Padova (INAF–OAPD), Vicolo dell'Osservatorio 5, I-35122, Padova Italy
[6] Space Telescope Science Institute, 3700 San Martin Boulevard, Baltimore, MD, 21218
[7] Department of Physics, University of Missouri, Kansas City, MO, USA
[8] Kavli Institute for Particle Astrophysics and Cosmology, Stanford, CA 94309, USA
[9] Department of Astronomy, University of Michigan, 500 Church Street, Ann Arbor, MI 48109, USA
[10] Department of Physics and Astronomy, Texas A&M University, College Station, TX, USA
[11] The School of Physics and Astronomy, University of Nottingham, Nottingham, UK
[12] Carnegie Observatories, Pasadena, CA 91101, USA

Understanding the history of the assembly of these galaxies throughout cosmic time is crucial to constrain models of galaxy evolution. The first generation of extremely massive ETGs ($M_\odot > 10^{11}$) is already in place at $z \sim 2.5$ (Guo et al. 2012); their number density dramatically increases during the $1 < z < 3$ epoch (Ilbert+10, Ilbert+13, Cassata+11, Brammer+11), followed by a milder evolution at $0 < z < 1$ (Bell et al. 2004; Faber et al. 2007; Pozzetti et al. 2010). The overall evolution of the ETGs depends strongly on stellar mass, following a "downsizing" pattern: more massive ETGs build up preferentially earlier than the less massive ones (Arnouts et al. 2007; Marchesini et al. 2009; Ilbert et al. 2010, 2013; Cassata et al. 2011, Brammer et al. 2011).

At the same time, the massive passive ETGs are found to have 3–5 times smaller sizes at $z > 1$ than in the local Universe (Daddi et al. 2005; Trujillo et al. 2007; Toft et al. 2007; Zirm et al. 2007; Cimatti et al. 2008; Van Dokkum et al. 2008; Buitrago et al. 2008), and thus they are 30–100 times denser. These results ignited a debate about the possible mechanism producing the size evolution: Naab, Johansson & Ostriker (2009) claim that the observed size evolution of passive ETGs can be explained by minor merger events, while Khochfar & Silk (2006) propose that the observed evolution can be explained by the variation of the amount of cold gas available during the major merger events that produce ETGs: the most massive ones formed at high–z, when major mergers were more gas rich than at later epochs. Although Lopez–Sanjuan et al. (2012) claimed that the

observed minor mergers at $0 < z < 1$ can account for up to 55% of the size growth of ETGs, Nipoti et al. (2012) claimed that minor and major mergers with spheroids are not sufficient to explain the observed size evolution between $z \sim 2.2$ and $z \sim 1.3$.

From a theoretical point of view, some key questions on the formation and evolution of ETGs are still open. We still do not know through which mechanism the ETGs accrete their mass: is it through major mergers at early epochs, as it is predicted by models of galaxy formation (Shankar et al. 2010; Shankar et al. 2011) or is it through the collapse of unstable disks, that have been shown to be numerous at $z \sim 2$ (Genzel et al. 2008; Förster–Schreiber et al. 2009)? What is the mechanism that shuts off the star formation in such objects, turning them into passively evolving ETGs? The dependence of the quenched ETG population on stellar mass and environment has been recently elucidated on phenomenological grounds (Peng et al. 2010, 2012), but what remain to be understood are the concrete physical mechanisms responsible for what is referred to as *mass quenching* and *environment quenching* in these studies.

In this paper we take advantage of the wealth of data available in the Chandra Deep Field South field, mainly gathered as a part of the GOODS and CANDELS surveys, to select a robust sample of passive ETGs at $1.2 < z < 3$, that we use to constrain the assembly of their mass content as function of the size, complementing and completing the analysis performed in Cassata et al. (2011; C11 hereafter). In particular, we dig into the passive population down to $M_* = 10^{10} M_\odot$ up to $z \sim 3$, a mass regime between 5 and 10 times below M^* (Ilbert et al. 2010).

Throughout the paper, we use a concordance cosmological model ($\Omega_\Lambda = 0.7$, $\Omega_m = 0.3$ and $H_0 = 70$ km s^{-1} Mpc^{-1}, we assume a Salpeter initial mass function (IMF; Salpeter et al. 1955) and we use AB magnitudes.

2. DATA AND SAMPLE SELECTION

The GOODS–South field is the one of the best studied parts of the sky, having been imaged with all the largest available telescopes (Hubble, Spitzer, VLT, Chandra, XMM, Herschel, CFHT). The GOODS HST Treasury Program (Giavalisco et al. 2004) provides ultradeep high–resolution images in B–, V–, i– and z–bands. Deep ground–based imaging in the U–band is provided by VIMOS/VLT for the CDFS (Nonino et al. 2009). Moreover, VLT/ISAAC imaged the CDFS in J–, H– and K–bands. Ultradeep Spitzer/IRAC imaging is also available in the 3.6, 4.5, 5.6 and 8.0 μm MIR channels and in the 24μm FIR one. The field has also been recently imaged with Herschel/PACS at 100 and 160 μm as a part of the GOODS/Herschel program (Elbaz et al. 2011). About 3000 spectroscopic redshifts are also available, among which 1200 are at $z > 1$ (Cimatti et al. 2008; Vanzella et al. 2008; Popesso et al. 2009; Kurk et al. 2013).

The Cosmic Assembly Near–infrared Deep Extragalactic Legacy Survey (CANDELS; Grogin et al. 2011; Koekemoer et al. 2011), the largest HST campaign ever undertaken, is collecting high resolution images in the F105W (Y–band), F125W (J–band) and F160W (H–band) filters for 5 of the most intensively studied extragalactic fields: namely, GOODS–South and North, EGS,
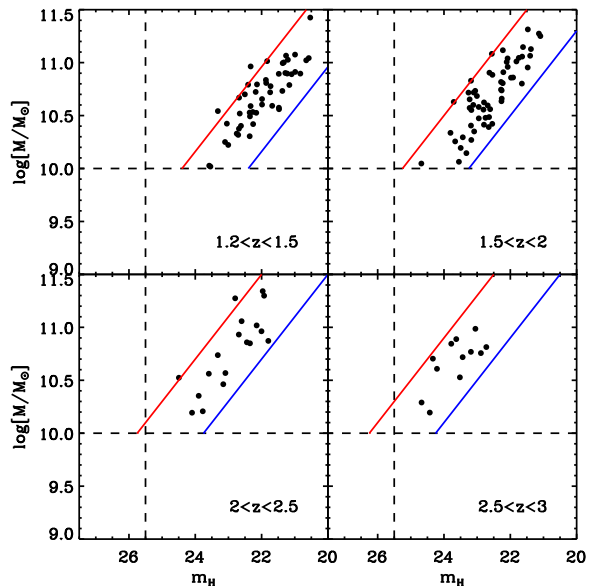

FIG. 1.— Stellar mass vs. AB magnitude in the WFC3/F160W H–band filter in four redshift bins: $1.2 < z < 1.5$, $1.5 < z < 2$, $2 < z < 2.5$ and $2.5 < z < 3$. The vertical dashed line at $m_{F160W} = 25.5$ indicates the magnitude at which the CANDELS H–band images are 80% complete, the dashed horizontal line at $M/M_\odot = 10^{10}$ shows the mass limit of our sample, the red and blue diagonal lines indicate, for each redshift bin, the stellar mass vs H–band magnitude relation for the reddest and bluest models available in our template grid.

UDS and COSMOS. In this paper we include the first 4 epochs of CANDELS observations in GOODS–S, that cover the central ~ 80 arcmin^2 of the GOODS–S field, for a total integration time of 2 orbits each in F125W (J–band) and F160W (H–band). We include as well the WFC3 observations taken as a part of the Early Release Science Program 2 (ERS2: GO 11359. PI: O'Connell; Windhorst et al. 2011), that cover an additional ~ 40 arcmin^2 area in the north part of the GOODS–S field, with integration times of 2 orbits in each of the F098M (Y–band), F125W (J–band) and F160W (H–band) filters. The final mosaics in Y–, J– and H–band were assembled using MultiDrizzle (Koekemoer et al. 2002), combining the data to a 0.06" pixel grid, and producing a PSF of ~ 0.16" in our resulting WFC3 images. The 1σ fluctuations of the sky for the ERS2 regions are 27.2, 26.6, and 26.3 AB $arcsec^2$ in the Y, J and H bands, respectively; for the 4–epoch CANDELS region, the 1σ fluctuations are 26.6 AB $arcsec^2$ for both the J– and H–bands.

We have built a multi–wavelength catalog using the TFIT procedures by Laidler et al. (2007), using the H–band as the detection image and including the U–band from VIMOS, the B, V, i and z bands from GOODS/ACS, the Y, J and H bands from CANDELS/WFC3 and the Ks band from VLT/ISAAC (Guo et al. 2013, in prep). This procedure allows us to match the point–spread function of images having different resolutions and to obtain homogeneous aperture magnitudes from the different images. The catalog includes about 11,000 objects brighter than $m_H = 25.5$,

4500 of which are at $1.2 < z < 3$, according to their spectroscopic or photometric redshift (see below).

We included the spectroscopic redshifts available in literature for the GOODS–S field (Vanzella et al. 2008; Cimatti et al. 2008; Popesso et al. 2009; Kurk et al. 2013) for 2232 objects, and we measured photometric redshifts for the remaining objects, using the PEGASE 2.0 templates (Fioc & Rocca–Volmerange 1997), following the same procedure in Guo et al. (2012).

We then fitted the SED from UV to 8 μm to the updated version of Bruzual&Charlot (2003, CB07) in order to get accurate measurements of stellar mass, E(B-V), age and SFR of the galaxies. In particular, we use a Salpeter IMF (Salpeter 1955) with lower and upper masses of 0.1 and 100 $M_\odot$, we apply the Calzetti law (Calzetti et al. 2000) to describe the dust extinction and we assume exponentially declining star formation histories SFR(t)$\propto e^{(-t/\tau)}$, where t is *age* (i. e. the time passed since the peak of the star formation) and τ is the characteristic time of the star formation event. Maraston et al. (2010) showed that these exponentially declining SFR models tend to overestimate the SFRs and underestimate stellar masses for star–forming galaxies at z∼2, while truncated exponentially increasing models give better results; however, the effect of such different SFH on passively evolving galaxies have not been conducted yet, and we defer this analysis to a forthcoming paper. In any event, these SED fits are only used to identify passively evolving galaxies.

We extracted a "parent" catalog of 1051 galaxies with $M_* > 10^{10}M_\odot$ and redshift $z > 1.2$, from which we selected only passive galaxies with Specific Star Formation Rate $SSFR < 10^{-2}$ Gyr^{-1} (332 galaxies). This SSFR limit is very restrictive: galaxies with $SSFR = 10^{-2}$ Gyr^{-1} would need 100 Gyr to double their stellar mass, if they continue to form stars at the present rate. We then eliminated all galaxies with a late-type morphology in the H–band WFC3 image (based on visual inspection, similarly to C11) and we also excluded galaxies detected in the Spitzer/MIPS 24μm and Herschel/PACS 100μm channels, ensuring that the SFR is lower than 10 $M_\odot yr^{-1}$ (Elbaz et al. 2011): the resulting sample of passive ETGs contains 107 galaxies. For the remaining of the paper, we define "ETGs" galaxies that are passive according to our criteria (SSFR and no detection in Herschel/Spitzer) and have a spheroidal morphology. 84% and 92% of the resulting 107 passive morphologically spheroidal ETGs have sersic indices $n > 2$ and $n > 2.5$, respectively (similarly to Bell et al. 2012): this ensures that our sample is not contaminated by quiescent disks as in van der Wel et al. (2011).

We used the GALFIT package (Peng et al. 2002) to fit the light profile in the $H - -$band (matching the rest–frame optical up to $z \sim 3$):

$$ I(r) = I_e exp \left\{ -b_n \left[\left(\frac{r}{r_e} \right)^{1/n} - 1 \right] \right\}, \qquad (1) $$

where $I(r)$ is the surface brightness measured at distance r, I_e is the surface brightness at the effective radius r_e and b_n is a parameter related to the Sérsic index n. For $n=1$ and $n=4$ the Sérsic profile reduces respectively to an exponential and deVaucouleurs profile.

Bulge dominated objects typically have high n values (e.g. $n > 2$) and disk dominated objects have n around unity. Ravindranath et al. (2006), Cimatti et al. (2008), Trujillo et al. (2007) and van der Wel et al. (2012) showed that GALFIT yields unbiased estimates of the Sérsic index and effective radius for galaxies with S/N> 10 and $r_e > 0.03''$, independently of the redshift of the source, thus demonstrating that the surface brightness dimming is not an issue for this kind of study.

The PSF was obtained in each passband needed by averaging well–exposed, unsaturated stars. We run GALFIT experimenting on various sizes of the fitting region around each galaxy, and with the sky either set to a pre–measured value or left as a free parameter. We verified that the sizes and Sérsic indices do not vary by more than 10% in the various cases. The values that we show throughout the paper were obtained with a free sky and 6×6 arcsec^2 fitting regions. Any close-by object detected by SExtractor within each fitting region was automatically masked out during the fitting procedure.

Figure 1 illustrates the completeness of our H–band selected catalog at different redshifts. In particular, we want to assess our ability to recover ETGs, which are very red because of the extremely constraining SSFR cut (SSFR$< 10^{-2}$), as a function of the stellar mass and redshift. The H–band image that we use in this work is 80% complete at least down to magnitude 25.5 for typical $z \sim 2$ spheroids with $R_e = 0.125''$ (Guo et al. 2013, in prep). We note that the 107 ETGs in our sample are detected at at more than 10σ in at least 4 filters blueward than the Balmer break, ensuring good photometric redshifts and mass determination.

In Fig. 1 we plot the stellar mass versus H–band magnitude for the reddest models in our grid (thus the hardest to detect), and we compare it with the distribution of our real ETGs at $1.2 < z < 3$. As expected, all the real galaxies lie right of the reddest model, meaning that, for a given stellar mass, they are brighter than the model. Since the H–band imaging is 80% complete down to magnitude $m_H \sim 25.5$ (Guo et al. 2013, in prep), we can conclude that our sample is complete down to stellar mass $M_\odot = 10^{10}$ up to $z \sim 3$. This implies that the scarcity of objects with $10^{10}M_\odot < M_* < 10^{10.5}$ in the two highest redshift bins of Fig. 1 is a real effect, and it is not due to mass incompleteness.

3. THE COLOR–MASS DIAGRAM AT $1.2 < Z < 3$

In Figure 2 we show the N_{UV} color–mass diagram in four redshift bins ($1.2 < z < 1.5$, $1.5 < z < 2$, $2 < z < 2.5$ and $2.5 < z < 3$) for the "parent" catalog (empty circles) and the ETGs (filled red circles). The absolute magnitudes for the N_{UV} and V filters are computed by interpolating the observed photometry at the location expected for the GALEX NUV 2500Å and Johnson V 5500Å, respectively. We separate the parent catalog in morphologically early– and late–types, based on the visual H–band morphology.

We observe a color bimodality up to $z \sim 2$, with the red peak dominated by ETGs and the blue distribution dominated by star forming late–type galaxies. At $z > 2$ the color distribution is unimodal, but still the red galaxies are on average more massive than the blue ones. In the two highest redshift bins, the bulk of objects displays blue colors and only a "tail" of red objects is present.
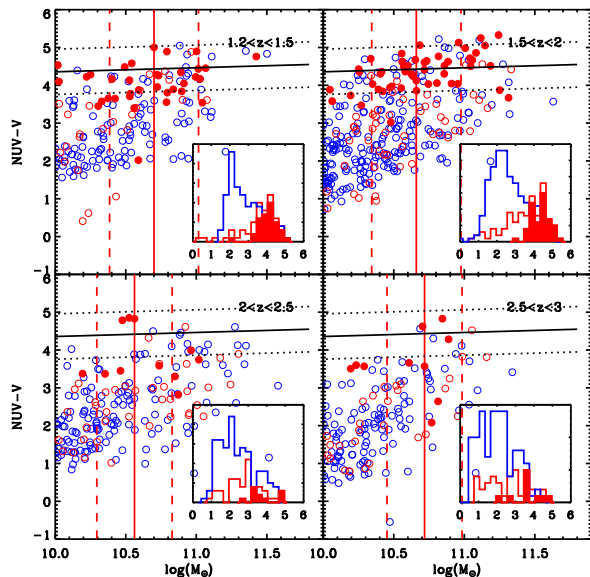
FIG. 2.— The N_{UV}–V color vs mass in the optical rest–frame for in four redshift bins: $1.2 < z < 1.5$, $1.5 < z < 2$, $2 < z < 2.5$ and $2.5 < z < 3$. The filled circles, red empty circles and blue empty circles represent the passive early–type galaxies (spheroidal morphology and SSFR$< 10^{-2}$), the morphologically early–type galaxies and the morphologically late–type galaxies, respectively. The black continuous and dashed lines show a fit to the ETGs in the first two bins combined. The insets show the color distribution in each bin, with the same color coding as the large figures. The red continuous and dotted lines show the median mass and scatter for the ETGs in the 4 redshift bins.

FIG. 3.— The mass size relation in the optical rest–frame for in four redshift bins: $1.2 < z < 1.5$, $1.5 < z < 2$, $2 < z < 2.5$ and $2.5 < z < 3$. In all bins, the grey filled region indicates the locus occupied by SDSS passive galaxies at $0 < z < 0.1$: the continuous line shows the median of the distribution, and the dashed lines contain 68% of the objects (from C11). Galaxies below the dotted line are defined as ultra–compact according to C11.

Only about 50% of the galaxies on the red sequence at such redshift are passive according to our criteria.

We note that the ETGs are the reddest and most massive objects, and that the red sequence is mostly populated by galaxies with $M_* > 10^{10.5} M_\odot$, at all redshifts. The average mass for ETGs in the four redshift bins is around $M_* = 10^{10.7} M_\odot$, with a dispersion of 0.2 dex. This shows that the most massive ETGs are the first to form at $z > 1.2$, and that, as cosmic time goes by, new low mass ETGs are formed. This result confirms earlier findings according to which the most massive galaxies are the first to be quenched (e.g., Bundy et al. 2006; Franceschini et al. 2006; Cimatti, Daddi & Renzini 2006) and is in qualitative agreement with the phenomenological model of Peng et al. (2010).

We see that there is a clear correlation between the morphology, the color and the star formation activity of the galaxies, at least up to $z = 2$: morphological early–type galaxies are typically red and passive; morphological late–types are blue and star forming. This is in good agreement with Whitaker et al. (2011), who found a red–sequence up to $z \sim 3.5$ (but the authors did not analyze the morphology of the galaxies on the red sequence), and Bell et al. (2012). These findings imply that the Hubble sequence, in the sense of a correlation between stellar mass, star formation properties and morphology, as observed in the local Universe, is already in place at $z \sim 3$. The mere existence of ETGs at $z \sim 3$ indicates that such objects formed and were quenched at even higher redshift; our estimate of the age is not accurate enough to
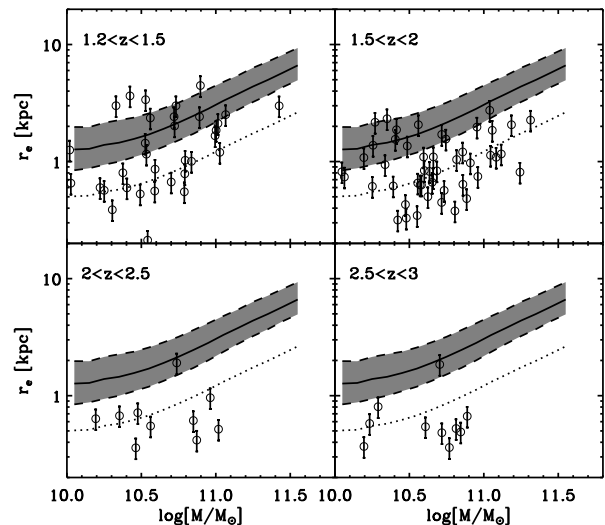
accurately age–date the bulk of the stellar component of such objects, but presumably they accreted the bulk of their mass about 1 Gyr prior to the observation, implying a formation redshift $z \sim 5$ (similar to Gobat et al. 2012).

4. THE MASS–SIZE RELATION FOR EARLY–TYPE GALAXIES AT $1 < Z < 3$

In Figure 3 we show the mass–size relation for the 107 massive and ETGs at $1.2 < z < 3$, in four redshift bins. The size is measured in the WFC3 H–band and matches the optical rest-frame in the whole redshift range. The plot shows also the mass–size relation for local ETGs drawn from the SDSS as derived by C11, according to whom galaxies below the SDSS local relation (the grey strip in Figure 3) are defined as *compact* ETGs (by definition, 17% of local ETGs are *compact*), and those more than 0.4 dex smaller than local counterparts of the same mass (the dotted line in Figure 3) are defined as *ultra–compact*. According to these definitions, compact and ultra–compact galaxies with a stellar mass $M_* = 10^{10.5} M_\odot$ have respectively sizes smaller than about 1 and 0.5 kpc. In our sample, at $2.5 < z < 3$, $2 < z < 2.5$, $1.5 < z < 2$ and $1.2 < z < 1.5$, respectively $\sim 90\%$ ($\sim 70\%$), $\sim 90\%$ ($\sim 60\%$), $\sim 80\%$ ($\sim 50\%$) and $\sim 70\%$ ($\sim 40\%$) of the ETGs are compact (ultra–compact) ETGs.

In Figure 4 we report the size as a function of the redshift for our sample of 107 massive ETGs at $1.2 < z < 3$, together with data at $0 < z < 1.2$ from C11: measurements for ETGs at $0.3 < z < 1.2$ are done in the z–band, that matches the optical rest–frame (see C11 for details); ETGs in the local universe ($0 < z < 0.1$) are drawn from the SDSS, and the measurements of their size are taken by the DR7 NYU Value–Added Galaxy Catalog (Blan-
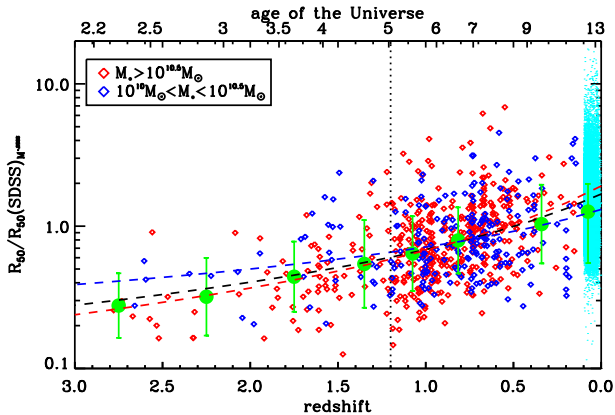
FIG. 4.— Evolution of the size for passive galaxies at $0 < z < 3$, normalized to the SDSS. The blue and red points represent ETGs with $M_* < 10^{10.5} M_\odot$ and with $M_* > 10^{10.5} M_\odot$, respectively. Measures at $z < 1.2$ (indicated by the dotted vertical line) come from C11. The green filled circles with their error bars represent the median size and scatter in bin of redshift. The black, blue and red dashed line show the best fit for all the ETGs, the ETGs with $M_* < 10^{10.5} M_\odot$ and ETGs with $M_* > 10^{10.5} M_\odot$, respectively.

FIG. 5.— *Top panel:* number density as a function of the age of the universe and redshift of all ETGs (black circles), normal size ETGs (blue diamonds), compact ETGs (green triangles) and ultra–compact ETGs (red squares). As a comparison, we report the data for passively evolving galaxies from Ilbert et al. (2010, cyan dotted line), Ilbert et al. (2013, purple dotted line), Brammer et al. (2011, black dotted line) and Moustakas et al. (2013, yellow filled star). We also report the lower limit estimate of the number density of compact ETGs by Valentinuzzi et al. (2010a, black upward arrow), fully compatible with our $z \sim 0$ estimate based on SDSS. *Bottom panel:* Fraction of passive galaxies that are also compact (green triangles) and ultra–compact (red squares), as a function of the age of the universe or the redshift.

ton et al. 2005, see C11 for details). Galaxy sizes are normalized to the average size of the SDSS ETGs with the same stellar mass. We also tried to normalize the size to the best–fit $R_e \propto M_\odot^{0.55}$ relation for each redshift (as for example in Cimatti, Nipoti & Cassata 2012), but the essence of the results discussed here did not change. In the same figure, we report the median normalized size for 8 redshifts, along with the scatter of the distribution: the $1 - \sigma$ standard deviation of the distribution is about 0.25 dex at all redshifts. We parameterize the evolution of the average size as $\langle r_e \rangle \propto (1 + z)^\alpha$, and we fitted the global population of ETGs, as well as ETGs with $M \lessgtr M^{10.5} M_\odot$ separately. To avoid the fit being completely driven by the $\sim 100{,}000$ SDSS galaxies at $0 < z < 0.1$, we exclude them from the fit. We find $\alpha = -1.29 \pm 0.10$ for the global population of ETGs, $\alpha = -0.89 \pm 0.16$ for ETGs with $M_* < M^{10.5} M_\odot$ and $\alpha = -1.50 \pm 0.12$ for ETGs with $M_* > M^{10.5} M_\odot$. This means that the size evolution is faster for high mass ETGs than for the low mass ones, in qualitative agreement with Ryan et al. (2012). Interestingly, this result does not change if only the C11 galaxies with $z < 1.2$ are included in the fit: we find $\alpha = -1.18 \pm 0.15$, $\alpha = -0.90 \pm 0.22$ and $\alpha = -1.33 \pm 0.18$ for all the ETGs, the ETGs with $M_* < M^{10.5} M_\odot$ and the ETGs with $M_* > M^{10.5} M_\odot$, respectively.

These values are in good agreement with results by Cimatti, Nipoti & Cassata (2012), who found $-1.25 < \alpha < -0.8$, and slightly smaller (in absolute value) than the value published by Damjanov et al. (2011), who found $\alpha = -1.62$. However, we stress that the sample used here (the 107 ETGs at $z > 1.2$ plus the ETGs at $z < 1.2$ by C11 is complete in mass down to $M_* = 10^{10} M_\odot$ up to $z = 3$, and it selected according to the same criteria at all redshift, thus being more homogeneous and complete than the ones used in these works, which are compilations of different samples published in literature.
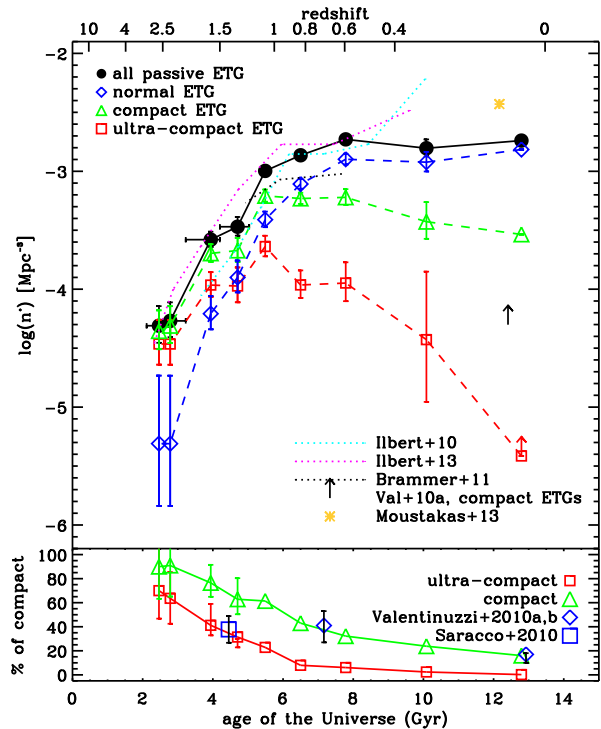
5. EVOLUTION OF THE NUMBER DENSITY IN PASSIVE GALAXIES AT $1 < Z < 3$

In Section 4 we saw that the mass–size relation of massive ETGs evolves fast with the redshift between $z \sim 3$ and $z \sim 1.2$: at $z > 2$ about 90% of the ETGs are compact (i.e. $1 - \sigma$ below the local relation), with that fraction dropping to 70% at $z \sim 1.2$. From Fig 4 we also learned that the average size of ETGs roughly doubles over the same redshift interval. The evolution of the average size of galaxies illustrated in in Figure 4 can be driven by two simultaneous processes: the size increase of each galaxy, possibly due to (minor) dry mergers (e.g., Naab et al. 2007; Nipoti et al. 2012; Oser et al. 2012) and to the appearance of new ETGs with a size distribution progressively shifted to larger sizes (Valentinuzzi et al. 2010a,b; Cassata et al. 2011; Newman et al. 2012; Poggianti et al. 2012; Carollo et al. 2013). We know that the number density of ETGs dramatically increases with cosmic time (i.e. Ilbert et al. 2010; Pozzetti et al. 2010), hence the size evolution can not be entirely attributed to the former mechanism, as it has been recently attempted by Oser et al. (2012). In order to try to constrain the relative importance of the two mechanisms, in this section we study the number density of ETGs of different physical

sizes as a function of the redshift and the cosmic time.

In Figure 5 we report the evolution of the number density of ETGs between $z = 3$ and $z = 1.2$ from this work, together with the same values at $0 < z < 1.2$ taken from C11. The only difference with C11 is that here we rebinned the data at $0 < z < 1.2$ in a slightly different manner, to better sample the range $0.1 < z < 0.7$, that covers about half of the age of the Universe and was sampled with only one bin in C11. We stress that the uniqueness of this work is that we exploit for the first time a sample of ETGs complete down to $M_* = 10^{10}M_\odot$, extending the analysis of C11 up to $z \sim 3$, when the Universe was just 2 Gyr old. We find that the number density of ETGs increases by a factor of 50 in a time span of only 3.5 Gyrs, between $z \sim 3$ and $z \sim 1$. Thus, the epoch $1 < z < 3$ is critical for the build–up of the number of massive ETGs, in good agreement with e.g., Ilbert et al. (2010, 2013) and with the phenomenological model of Peng et al. (2010). The number density of ETGs then further doubles in the 10 Gyr time span between $z \sim 1$ and $z \sim 0$, which is primarily due to the increase of low–mass ETGs (e.g., Ilbert et al. 2010; Franceschini et al. 2006; Cimatti, Daddi & Renzini 2006; Peng et al. 2010). Our measurements for the number density evolution of the global population of ETGs is in good agreement with Ilbert et al. (2010, 2013) and Brammer et al. (2011), obtained with much larger and less cosmic variance prone samples.

We see that the first ETGs to appear at $z \sim 3$ are virtually all compact or ultra–compact. The very rapid increase in the number density of the global population of ETG between $z \sim 3$ and $z \sim 1$ is caused by the fast and steady increase of the number densities of all normal, compact, and ultra–compact ETGs. By $z \sim 1.5$, the normal ETGs become more numerous than the ultra–compact, and at $z \sim 1$ they are the most common ETGs, exceeding the number of compact ETGs.

After $z \sim 1$, the number density of normal ETGs keeps steadily increasing, albeit at a modest rate. At the same time, the evolution of compact and ultra–compact ETGs decouples from that of the large ETGs, with their number density steadily decreasing. In the local Universe, the compact galaxies are (by definition, as they are defined to be 1-σ below the local relation) 17% of the global population of ETGs, and the ultra–compact formally disappear almost completely by $z \sim 0$. However, it has been argued that the SDSS database may be biased against very compact galaxies (Scranton et al. 2002; Shih & Stockton 2011; Valentinuzzi et al. 2010a; Carollo et al. 2013). We note that our estimate of the number density of compact ETGs at $z \sim 0$ is ~ 5 times higher than the lower limit determined by Valentinuzzi et al. (2010a), thus formally in agreement, and that our new point at $z \sim 0.4$ seems to confirm the mild decrease. From $z \sim 1$ to $z \sim 0$ the number density of compact ETGs decreases by a factor of around 2. The picture is less clear for the ultra-compact ETGs: the SDSS imaging does not offer enough spatial resolution to identify ultra-compact ETGs, and thus we indicate the number density of ultra-compact ETGs as a lower limit in Figure 5. The new point at $z \sim 0.4$ seems to support the fast decrease of the the number density of ultra-compact ETGs at $0 < z < 1$, but the large error bar does not help to unambiguously fix the issue. In the end, the evolution seems to be strongly

size–dependent, with a faster decrease for smaller ETGs, even though we can not draw any strong conclusion due to the $z \sim 0$ uncertainties. This differential evolution is in quite good agreement with recent results by Carollo et al. (2013), who found a even milder decrease of the number density of ETGs with sizes smaller than 2 kpc (that is slightly larger than our "compactness" definition: according to our definition, ETGs of $M_* = 10^{10.5}M_\odot$ are compact if their size is smaller than 1 kpc).

6. DISCUSSION AND CONCLUSIONS

In this paper we analyzed a sample of passive (SSFR$<$ $10^{-2}Gyr^{-1}$) and massive ($M_* > 10^{10}M_\odot$) ETGs at $1.2 < z < 3$. The deep H–band imaging ensures that the sample is complete down to $M_* = 10^{10}M_\odot$, about an order of magnitude below M^* (Ilbert et al. 2010) and allows us to study the morphology of our galaxies in the optical rest–frame up to $z \sim 3$. Moreover, the dense multiwavelength coverage ensures robust redshift measurements (for the objects without a spectroscopic redshift), accurate mass and star formation activity determinations. The Herschel and Spitzer ancillary data allowed us to reinforce the passivity selection based on the SED fitting procedure.

The key finding of this paper are: 1. the identification up to $z \sim 3$ of passive and massive ETGs, that dominate the red sequence (well defined up to $z \sim 2$, less clear at $2 < z < 3$, see Figure 2); 2. the accurate determination, with the evolution of average size for ETGs at $0 < z < 3$, reported in Figure 4; 3. the robust determination of the differential evolution of the spatial abundance of massive, i.e. stellar mass $M_* > 10^{10}$ $M_\odot$, passive galaxies as a function of redshift and as a function of the their size, a proxy of their average projected central stellar density, shown in Figure 5.

At high redshift, i.e. $z \sim 3$, the size distribution of ETGs is heavily tilted toward small sizes, and massive and passive galaxies are predominantly high–stellar density systems. This implies that the mechanism through which these galaxies accrete their mass and eventually become passive at those early epochs leaves a remnant that is very compact (Cimatti et al. 2008). Many different mechanisms leading to the formation of compact remnants have been proposed in literature: Dekel et al. (2009) argued that disk instabilities lead to the formation of compact remnants; Hopkins et al. (2008), Wuyts et al. (2010) and Bournaud et al. (2011) showed that gas–rich mergers can form compact galaxies; Johansson, Naab, & Ostriker (2012) proposed that compact galaxies can formed by in situ star formation driven by cold flows.

By $z \sim 1$ the abundance of small ETGs reaches its peak, followed by a decline, apparently faster for the ultra–compact than for the compact ones (see Section 5 and discussion of the uncertainties for $z < 0.5$). Apparently, whatever set of mechanisms was producing ultra–compact passive galaxies at $1 \lesssim z \lesssim 2.5$ is not working anymore at later epochs. Moreover, the size distribution of the new ETGs that become passive between $z \sim 1$ and $z \sim 0$ is gradually moving towards larger sizes, implying that the mechanism through which star formation is quenched in these massive ETGs acts in such a way as to leave larger quenched remnants as (cosmic) time goes by, a tendency which accelerates at $z < 1$. This may be a

natural consequence of the *inside–out* growth of the disks (a widely entertained notion, Samland & Gerhard 2003; Brook et al. 2006; Muñoz–Mateos et al. 2011), with such disks being the likely precursors to passive ETGs. So, bigger disks would leave bigger ETG *remnants*.

In the $0 < z < 1$ epoch the average size of the ETGs steadily increases (see Figure 4). This evolution might be due to two different mechanisms (or a mix of the two): on one hand, the individual ETGs increase in size, by minor merging or accretion; on the other hand new already large ETGs, that never passed through the compact or ultra–compact phase, appear. In this respect, the evolution of the number densities of ETGs of different sizes, constrained in Figure 5, can help to weigh the relative importance of two mechanisms. In particular, even assuming that all the disappearing compact and ultra–compact ETGs are transformed in ETGs of normal size and density, in a cascade of merging and interactions to form normal–sized galaxies (e.g. Huang et al. 2012), Figure 5 shows that they are not numerous enough to support the increase of the total number of normal ETGs observed over the same time interval. In fact, between $z \sim 1$ and $z \sim 0$ the number density all ETGs increases by about $\sim 0.8 \times 10^{-3} Mpc^{-3}$, while the number density of compact ETGs that disappear is only $\sim 0.3 \times 10^{-3} Mpc^{-3}$. This implies that the observed rate at which compact galaxies disappear can not sustain the observed increase of the number of normal ETGs; thus the growth of the individual ETGs is not the dominant mechanism causing the average size of ETGs to increase (Fig. 4), in agreement with Carollo et al. (2013).

At the same time, the decrease of the number density of compact and ultra–compact ETGs between $z \sim 1$ and $z \sim 0$ indicates that a fraction of these galaxies either become active, because of a sudden refurbishment of fresh gas, or –more likely– they grow in size, via minor merging or smooth accretion, becoming normal–sized ETGs.

Before concluding, we also wish to comment on the cosmic rise and fall of the ultra–compact passive galaxies that this paper has documented. The extreme compactness and large stellar mass of these galaxies argue against hierarchical merging of stellar systems as the primary mechanism for the assembly of their stellar mass (Giavalisco et al. in prep.). Rather, it is likely that they emerged in their final state after the quenching of star–forming galaxies of the same size and density. In this case the rise and fall of ultra–compact ETGs are the result of four different processes: 1) the rate at which ultra–compact star–forming galaxies form in this mass range (roughly $M_* > 10^{10}$ M$_\odot$) ; 2) the rate at which they are destroyed before they quench, i.e. they are transformed from ultra–compact into galaxies of lower density by merging and interactions; 3) the rate at which the ultra–compact star–forming galaxies shut down star formation and become passive; 4) the rate at which the ultra–compact passive galaxies are transformed into galaxies of lower stellar density by merging and interactions. 1) and 2), although not directly constrained by this work, define the "reservoir" of compact star–forming galaxies from which compact ETGs can form; the effects of mechanism 3) and 4) in shaping the number density evolution of compact ETGs has been extensively discussed in this paper.

Interestingly, Wuyts et al. (2011) and

Barro et al. (2013) identified a rich population of compact star forming galaxies at $1.5 < z < 3$, whose number densities and physical properties are compatible with being the progenitors of the compact and ultra–compact ETGs. The authors speculate that those compact star forming galaxies are formed from a gas–rich process (merger or disk instabilities) that at first induce a compact starburst and then feed an AGN, which quenches the star formation turning these objects into compact ETGs. They find that these compact star forming objects are very rare at $z < 1.5$, supporting our conjecture that after that epoch the mechanism through which ETGs are formed produce a large remnant. However, the definition of ETGs in Barro et al. (2013), as well as the definition of which star forming galaxies can transform in ETGs differ from ours. So, we looked for progenitors of our ETGs in a companion paper, Williams et al. (2013, in preparation): we have identified a sample of compact star forming galaxies which may be progenitors of our high–redshift passive sample, (which represent some of the first ETGs to appear in the universe). This sample have consistent SFRs and stellar masses with our ETGs, and are evolutionarily consistent assuming physically motivated SFHs. This sample demonstrates that massive and active enough compact SF galaxies exist at $z > 3$ to account for the number density of compact ETGs presented here, assuming mass buildup by purely in–situ star–formation, further justifying the evolutionary link between compact SF and compact passive galaxies.

To summarize, our main findings are:

- We find that at $1 < z < 3$ the passively evolving ETGs are the reddest and most massive objects in the Universe. This implies that an embryo of the Hubble Sequence, in the sense of a correlation between morphology, mass, color and star–formation activity of galaxies, is already in place at $z \sim 3$. We observe a scarcity of ETGs with $M_* < 10^{10.5} M_\odot$, with the majority of our ETGs having $M_* > 10^{10.5} M_\odot$. Since we accurately set our mass completeness to $M_* = 10^{10} M_\odot$, we can conclude that that scarcity is not due to an observational bias. Hence, at $z > 1.2$ the mechanism producing ETGs leaves a remnant that is preferentially very massive. This result reinforces previous claims for a "downsizing" pattern of the mass assembly of ETGs. A possible interpretation is that at that early epoch the process that suddenly quenches the star–formation activity in some objects, transforming them into passively evolving ETGs, is effective preferentially for objects with stellar mass above $M_* = 10^{10.5} M_\odot$. This result is in qualitative agreement with Peng et al. (2010), who highlighted the prominent role of mass quenching at high redshift.

- We measure a significant evolution of the mass–size relation of ETGs from $z \sim 3$ to $z \sim 1$, with the average size of galaxies increasing by roughly a factor of ~ 2 over this redshift interval, corresponding to 3 Gyrs of cosmic time. The evolution of the size of ETGs is faster for galaxies with $M_* > 10^{10.5} M_\odot$ than for those with $M_* < 10^{10.5} M_\odot$. About 90% (70%) of the ETGs at $z > 2$

are compact (ultra–compact). We find that the average size of ETGs between $z \sim 3$ and $z \sim 0$ evolves with the redshift following a simple power law $r_e \sim (1+z)^\alpha$, with $\alpha = -1.18 \pm 0.15$. If ETGs with $M \lesssim M^{10.5} M_\odot$ are fitted separately, we find a marginally steeper power α for the most massive ETGs ($\alpha = -1.33 \pm 0.18$), indicating a faster size evolution.

- We witness the build up of the most massive ETGs, with their number density increasing by 50 times between $z \sim 3$ and $z \sim 1$. We find that 90% of ETGs at $z > 2$ are compact or ultra–compact, indicating that the event through which such first ETGs accrete their mass leaves a remnant that is very compact. As the cosmic time goes by, new ETGs tend to be larger and larger, with the "normal" sized ETGs (meaning those objects with sizes comparable to the local ETGs of the same mass) becoming the most common ETGs at $z \sim 1$. At $z > 1$ the mechanisms creating new ultra–compact ETGs prevail on those destroying them (merging, smooth accretion), resulting in a net increase of their number density; at $z < 1$ the balance between such mechanisms inverts, with the processes decreasing the stellar density of ultra–compact galaxies finally prevailing. Thus, the number density of compact passive ETGs starts decreasing, although the measure of such decrease to $z = 0$ remains quite uncertain. Still, such decrease would not account for the increased number of "normal–size" galaxies, even if all the compact, passive ETGs at $z = 1$ were to disappear by $z = 0$, Therefore, the evolution of the average size of ETGs at $0 < z < 1$ is mainly due to the appearance of newly quenched ETGs that are born large, rather than to the size increase of individual galaxies.

REFERENCES

Arnouts, S., Walcher, C. J., Le Fèvre, O., et al., 2007, A&A, 476, 137

Baldry, Ivan K., Glazebrook, Karl, Brinkmann, J., et al., 2004, ApJ, 600, 681

Barro, G., Faber, S. M., Perez–Gonzalez, P. G., et al., 2012, ApJ, 765, 104

Bell, E. F., Wolf, C., Meisenheimer, K., et al., 2004, ApJ, 608, 752

Bell, E. F., van der Wel, A., Papovich, C., et al., 2012, ApJ, 753, 167

Blanton, M. R., Schlegel, D. J., Strauss, M. A., et al. 2005, AJ, 129, 2562

Borch, A., Meisenheimer, K., Bell, E. F., et al. 2006, A&A, 453, 869

Bournaud, F., Chapon, D., Teyssier, R., et al., 2011, ApJ, 730, 4

Brammer, G. B., Whitaker, K. E., van Dokkum, P. G., et al., 2011, ApJ, 739, 24

Brook, C. B., Kawata, D., Martel, H., et al., 2006, ApJ, 639, 126

Bruzual, G., & Charlot, S., 2003, MNRAS, 344, 1000

Buitrago, F., Trujillo, I., Conselice, C. J., et al. 2008, ApJ, 687, L61

Bundy, K., et al. 2006, ApJ, 651, 120

Carollo, C. M., Bschorr, T. J., Renzini, A., et al., 2013, submitted to ApJ, [astro-ph/302.5115]

Cassata, P., Cimatti, A., Franceschini, A., et al. 2005, A&A, 357, 903

Cassata, P., Cimatti, A., Kurk, J., et al. 2008, A&A, 483, L39

Cassata, P., Giavalisco, M., Guo, Yicheng, et al. 2010, ApJ, 714, L79

Cimatti, A., Daddi, E., & Renzini, A., 2006, A&A, 453, 29

Cimatti, A., Cassata, P., Pozzetti, L., et al. 2008, A&A, 482, 21

Cimatti, A., Nipoti, C., & Cassata, P., 2012, MNRAS, 422, 62

Daddi, E., et al. 2005, ApJ, 626, 680

Damjanov, I., Abraham, R. G., Glazebrook, K., et al., ApJ, 739, 44

Elbaz, D., Dickinson, M., Hwang, H. S., et al., 2011, A&A, 533, 119

Faber, S. M., Willmer, C. N. A., Wolf, C., et al., 2007, ApJ, 665, 265

Fioc, M., & Rocca–Volmerange, B., 1997, A&A, 326, 950

Förster–Schreiber, N. M., et al., 2009, 706, 1364

Franceschini, A., Rodighiero, G., Cassata, P., et al. 2006, A&A, 453, 397

Genzel, R., Burkert, A., Bouché, N., et al., 2008, ApJ, 687, 59

Giavalisco, M., Dickinson, M., Ferguson, H. C., et al. 2004, ApJ, 600, 103

Gobat, R., Strazzullo, V., Daddi, E., et al., 2012, ApJ, 759, 44

Grogin, N. A., Kocevski, D., D., Faber, S. M., et al., 2011, ApJ, 197, 35

Guo, Y., Giavalisco, M., Cassata, P., et al., 2012, ApJ749, 149

Hopkins, P. F., Hernquist, L., Cox, T., et al., 2008, ApJ, 688, 757

Hopkins, P. F., Bundy, K., Murray, N., et al., 2009, MNRAS, 398, 898

Huang, Song, Ho, L. C., Peng, C. Y., et al., 2012, ApJin press, [astro-ph/1212.2639]

Ilbert, O., Salvato, M., Le Floc'h, E., et al. 2010, ApJ, 709, 644

Ilbert, O., McCracken, H. J., Le Fèvre, O., et al. 2013, submitted to A&A, [astro-ph/1301.3157]

Johansson, P. H., Naab, T., Ostriker, J. P., ApJ, 754, 115

Khochfar, S., & Silk, J., 2006, ApJ, 648, L21

Koekemoer, A. M., et al., 2002, HST Calibration Workshop (eds. S. Arribas, A. M. Koekemoer, B. Whitmore, Baltimore: STScI), 337

Koekemoer, A. M., Faber, S. M., Ferguson, H. C., et al., 2011, ApJ, 197, 36

Kurk, J., Cimatti, A., Daddi, E., et al., 2013, A&A, 549, 63

Laidler, V. G., Papovich, C., Grogin, N. A., et al., 2007, PASP, 119, 1325

López-Sanjuan, C., Le Fèvre, O., Ilbert, O., A&A, 548, 7

Maraston, C., Pforr, J., Renzini, A., et al. 2010, MNRAS, 407, 830

Marchesini, D., Van Dokkum, P. G., Förster-Schreiber, N. M., 2009, et al., ApJ, 701, 1765

Muñoz–Mateos, J. C., Boissier, S., Gil de Paz, A., et al., 2011, et al., ApJ, 731, 10

Naab, T., Johansson, P. H., Ostriker, J. P., et al., 2007, ApJ, 658, 710

Naab, T., Johansson, P. H., & Ostriker, J. P., 2009, ApJ, 699, 178

Newman, A. B, Ellis, R. S., Bundy, K., & Treu, T., 2012, ApJ, 746, 162

Nipoti, C., Treu, T., Leauthaud, A., et al., 2012, MNRAS, 422, 1714

Nonino, M., Dickinson, M., Rosati, P., et al. 2009, ApJS, 183,244

Oser, L., Naab, T., Ostriker, J. P., et al., 2012, ApJ, 744, 63

Peng, C. Y., Ho, L. C., Impey, C. D., et al. 2002, AJ, 124, 266

Peng, Y., Lilly, S. J., Kovac, K., et al. 2010, ApJ, 721, 193

Peng, Y., Lilly, S. J., Renzini, A., & Carollo, M., 2012, ApJ, 757, 4

Poggianti, B. M., Calvi, R., Bindoni, D., et al., 2012,ApJ, 762, 77

Popesso, P., Dickinson, M., Nonino, M., et al. 2009, A&A, 494, 443

Pozzetti, L., Bolzonella, M., Zucca, E., et al., 2010, A&A, 523, 13

Ryan, R. E. Jr., McCarthy, P. J., Cohen, S. H., et al. 2012, ApJ, 749, 53

Ravindranath, S., Giavalisco, M., Ferguson, H. C., et al. 2006, ApJ, 652, 963

Renzini, A., 2006, ARA&A, 44, 141

Sales, L. V., Navarro, J. F., Theuns, T., et al. 2012, MNRAS, 423, 1544

Salpeter, E. E., 1955, ApJ, 121, 161

Samland, M., & Gerhard, O. E., 2003, A&A, 399, 961

Shankar, F., Marulli, F., Bernardi, M., et al. 2010, MNRAS, 405, 948

Shankar, F., Marulli, F., Bernardi, M., et al. 2011, submitted to MNRAS, [astro-ph/1105.6043]

Shih, H., & Stockton, A., 2011, ApJ, 733, 45

Toft, S., van Dokkum, P., Franx, M., et al. 2007, ApJ, 671,285

Trujillo, I., Feulner, G., Goranova, Y., et al. 2006, MNRAS, 373, L36

Trujillo, I., Conselice, C. J., Bundy, K., et al. 2007, MNRAS, 382, 109

Van Dokkum, P. G., Franx, M., Kriek, M., et al. 2008, ApJ, 677, L5

Valentinuzzi, T., Fritz, J., Poggianti, B., et al. 2010, ApJ, 712, 226

Valentinuzzi, T., Poggianti, B. M., Saglia, R. P., et al. 2010, ApJ, 721, L19

van der Wel, A., Rix, H.-W., Wuyts, S., et al., 2011, ApJ, 730, 38

van der Wel, A., Bell, E. F., Häussler, B., et al., 2012, ApJS, 203, 24

Van Dokkum, P. G., Whitaker, K. E., Brammer, G., et al. 2010, ApJ, 709, 1018

Vanzella, E., Cristiani, S., Dickinson, M., et al. 2008, A&A, 478, 83

Windhorst, R. A., Cohen, S. H., Hathi, N. P., et al. 2011, ApJS, 193, 27

Whitaker, K. E., Labbé, I., van Dokkum, P. G., et al. 2011, ApJ, 735, 86

Wuyts, S., Cox, T., Hayward, C. C., et al. 2010, ApJ, 722, 1666

Wuyts, S., Förster Schreiber, N. M., van der Wel, A., et al. 2011, ApJ, 742, 96

Zirm, A. W., van der Wel, A., Franx, M., et al. 2007, ApJ, 656, 66